General Disclaimer

One or more of the Following Statements may affect this Document

- This document has been reproduced from the best copy furnished by the organizational source. It is being released in the interest of making available as much information as possible.

- This document may contain data, which exceeds the sheet parameters. It was furnished in this condition by the organizational source and is the best copy available.

- This document may contain tone-on-tone or color graphs, charts and/or pictures, which have been reproduced in black and white.

- This document is paginated as submitted by the original source.

- Portions of this document are not fully legible due to the historical nature of some of the material. However, it is the best reproduction available from the original submission.

NASA TECHNICAL MEMORANDUM

NASA TM X- 72717

NASA TM X-72717

(NASA-TM-X-72717) ACCURACY OF ESTIMATING THE MASSES OF PHOBOS AND DEIMOS FROM MULTIPLE VIKING ORBITER ENCOUNTERS (NASA) 22 p HC $3.25 CSCL 03B

N75-27987

Unclas
G3/91 28088

ACCURACY OF ESTIMATING
THE MASSES OF PHOBOS AND DEIMOS
FROM MULTIPLE VIKING ORBITER ENCOUNTERS

BY

Robert H. Tolson and Mary L. Mason

July 1975

NATIONAL AERONAUTICS AND SPACE ADMINISTRATION
LANGLEY RESEARCH CENTER, HAMPTON, VIRGINIA 23665

1. Report No.	2. Government Accession No.	3. Recipient's Catalog No.
NASA TM X-72717		

4. Title and Subtitle	5. Report Date
Accuracy of Estimating the Masses of Phobos and Deimos from Multiple Viking Orbiter Encounters	July, 1975
	6. Performing Organization Code

7. Author(s)	8. Performing Organization Report No.
Robert H. Tolson and Mary L. Mason	
	10. Work Unit No.

9. Performing Organization Name and Address	11. Contract or Grant No.
NASA Langley Research Center Hampton, VA 23665	
	13. Type of Report and Period Covered

12. Sponsoring Agency Name and Address	14. Sponsoring Agency Code
National Aeronautics and Space Administration Washington, DC 20546	Technical Memorandum

15. Supplementary Notes

16. Abstract

This paper addresses the problem of estimating the masses of Phobos and Deimos from Doppler and onboard optical measurements during the Viking extended mission. A Kalman filter is used to analyze the effects of gravitational uncertainties and non-gravitational accelerations. These accelerations destroy the dynamical integrity of the orbit and multi-batch or limited memory filtering is preferred to single batch processing. Optical tracking is essential to improve the relative orbit geometry. The masses can be determined to about 10% and 25% respectively for Phobos and Deimos, assuming satellite densities of about 3 gr/cm^3.

17. Key Words (Suggested by Author(s)) (STAR category underlined)	18. Distribution Statement
Mar's moons, Mar's natural satellites, PHOBOS, DEIMOS, Viking '75, mass determination, orbital mechanics, mission design	unclassified - unlimited

19. Security Classif. (of this report)	20. Security Classif. (of this page)	21. No. of Pages	22. Price*
unclassified	unclassified	22	$3.25

*Available from { The National Technical Information Service, Springfield, Virginia 22151
STIF/NASA Scientific and Technical Information Facility, P.O. Box 33, College Park, MD 20740

ACCURACY OF ESTIMATING THE MASSES OF PHOBOS AND DEIMOS FROM MULTIPLE VIKING ORBITER ENCOUNTERS

Robert H. Tolson and Mary L. Mason

This paper addresses the problem of estimating the masses of Phobos and Deimos from Doppler and onboard optical measurements during the Viking extended mission. A Kalman filter is used to analyze the effects of gravitational uncertainties and non-gravitational accelerations. These accelerations destroy the dynamical integrity of the orbit and multi-batch or limited memory filtering is preferred to single batch processing. Optical tracking is essential to improve the relative orbit geometry. The masses can be determined to about 10% and 25% respectively for Phobos and Deimos, assuming satellite densities of about 3 gr/cm^3.

INTRODUCTION

Two Viking spacecraft will be placed into orbits about Mars in the summer of 1976. Each spacecraft will separate into an orbiter (VO) and a lander (VL). Upon separation, the VL will perform a propulsive maneuver, causing the spacecraft to enter the atmosphere and soft land on the surface of Mars. The orbiters will perform experiments to support the landers and act as relay stations to return VL scientific data to the Earth.

The spacecraft orbital parameters are largely determined by the landing sites on Mars. For the nominal landing sites the orbital geometry is shown in Fig. 1. Both orbiters have periods synchronous with the rotational period of Mars and periapsis altitudes of 1500 km. The orientation elements are given in July for the A spacecraft and August for the B spacecraft. The precession of the VO-A spacecraft due to Mars planetary oblateness provides a

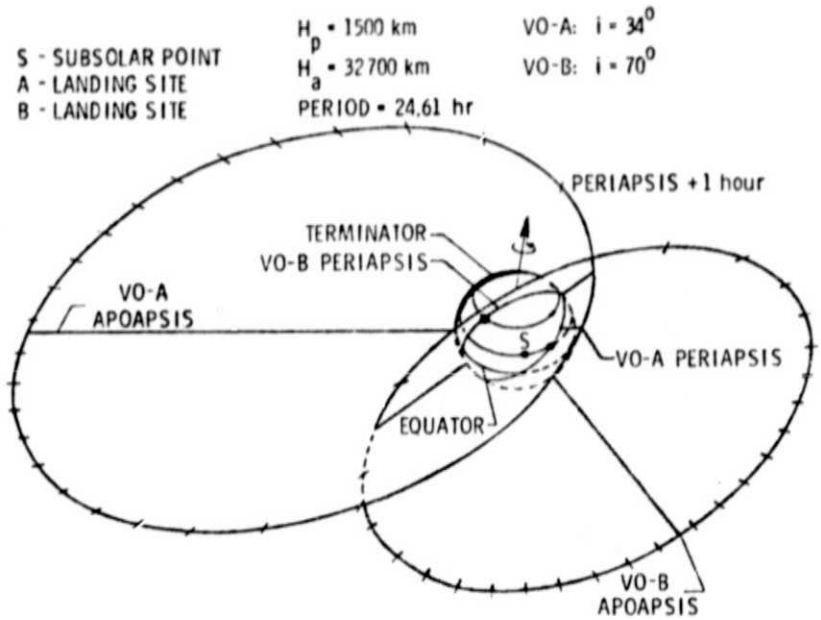

Figure 1. Inertial orbits of the Viking orbiters.

unique opportunity to explore the natural satellites Phobos and Deimos from distances measured in tens of kilometers[1]. The geometric aspects of this opportunity are shown in Fig. 2. The plane of the figure is the Mars equatorial plane. The points where the spacecraft ascends and descends through the equatorial plane are indicated for a number of orbits. Initially, the descending intersection point is between the orbital paths of the natural satellites and the ascending intersection point is inside the Phobos orbit. However, nodal regression and apsidal precession cause both of these points to move toward the Phobos orbital path. In January and March the spacecraft will pass within 10 km of the Phobos orbit. As precession continues, the ascending intersection point moves outward so that in late 1977 VO-A will

pass within 50 km of the Deimos orbital path. Thus, with proper phasing, the spacecraft can be maneuvered to pass very close to both natural satellites. Since phasing can be performed over relatively long time periods, it can be accomplished for very small propulsive cost. For the January and March

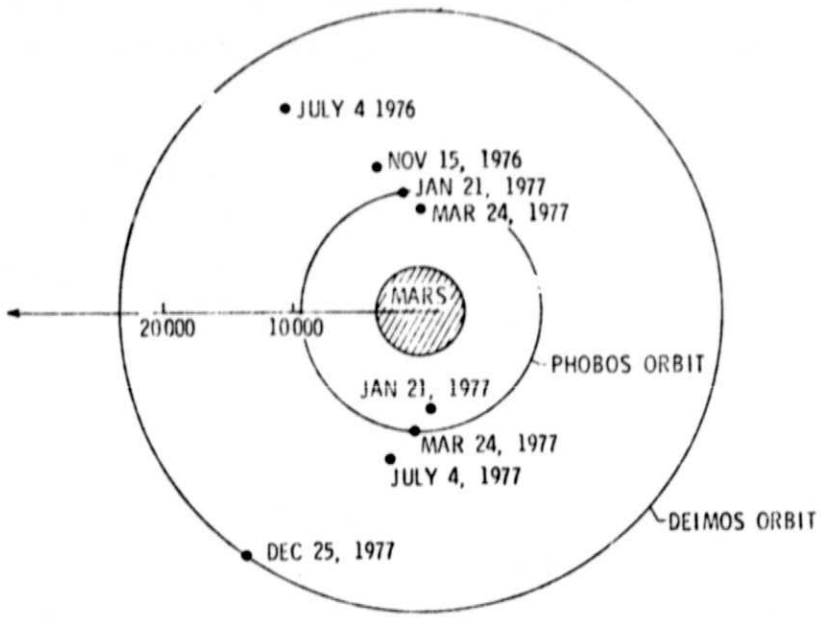

Figure 2. Phobos and Deimos inertial encounter geometry for VO-A

encounters, it is also possible to establish a 1 to 3 ratio between the spacecraft and Phobos orbital period for about 20 m/s of propulsive expenditure[1], which is well within the spacecraft capability. Thus, repeated encounters at close distances are possible. The Deimos encounter opportunity requires more propulsive expenditure to maximize the number of close encounters, because the Deimos orbital period (30.3 hrs) is substantially different from the nominal VO orbital period. However, other commensurable period ratios, such as 5 to 4, can be established for a few meters per second.

The final encounter geometry will be designed to accomplish a number of scientific objectives, among which is the determination of the natural satellite masses. The mass of Phobos is a significant geophysical parameter, since it can be related directly to internal properties of Mars. In addition, if the volumes of the natural satellites can be determined, knowledge of the masses can be used to infer density and hence, composition. It is expected that a combination of Mariner 9 and Viking imagery data will produce satellite volumes with an accuracy of about $10\%^2$. Thus, mass determination to less than 10% is desirable.

This paper addresses the problem of determining the masses of the natural satellites from the VO-A tracking data and from imagery data. This parametric analysis of the masses of Phobos and Deimos considers various approach geometries, dynamic noise levels, and data processing methods.

ERROR ANALYSIS

Dynamic Model. The dynamic model for an error analysis does not demand the fidelity of a data processing model. To analyze close encounters of Phobos or Deimos it is only necessary that the spacecraft and satellite orbital motions include the dominant perturbative effects. Perturbations to the two body orbital motion are due to the non-central part of the Martian gravitational field, third body forces, radiation pressure, drag, and gas leaks. The dominant gravitational perturbation is the oblateness or the J_2 term, which to first order produces the apsidal precession and nodal regression discussed above. Tesseral harmonics, third body forces, etc., produce variations in the orbit which will not substantially effect the relative geometry. Thus, the spacecraft orbital motion is modeled as a uniformly precessing conic according to the classical formulas:

$$\dot{\Omega} = -3/2\ n\ J_2\ \cos i\ (R/a)^2/(1-e^2)^2$$

$$\dot{\omega} = 3/2\ n\ J_2\ (2-5/2\ \sin^2 i)(R/a)^2/(1-e^2)^2$$

The orbital elements, the secular rates, and other physical parameters for Phobos and Deimos used in this analysis are given in Table 1. The orbital parameters[3] and mean diameters[4] were determined from Mariner 9 optical data. More detailed orbital representations are available[3,5,6]; however, a first order model is more than adequate for this analysis. The gravitational constant assumes a density of about 3 gr/cm^3.

Observational Model. The Viking spacecraft has two video imaging systems which have a small amount of image overlap and parallel optical axes. Each image is composed of an array of about 1000 × 1000 picture elements or pixels. These systems are calibrated with star images during interplanetary cruise to measure image distortion and system alignment. This calibration assures an accuracy of all subsequent pictures or picture pairs to the pixel level of about 0.025 milliradians.

The optimum utilization of this system for determining the orbits of the natural satellites is to simultaneously image the satellite with one system

Table 1

PHYSICAL PARAMETERS OF PHOBOS AND DEIMOS ON NOVEMBER 11, 1971

	Phobos	Deimos
a, km	9378.53±.01	23458.91±.03
e	0.0150±.0001	0.0008±.0001
Mo, deg	311.82±.36	232.6±7.
i, deg	1.04±.01	2.79±.02
ω, deg	269.9±.9	235.6±7.
Ω, deg	100.5±.8	10.9±.2
n, deg/day	1128.4069	285.1438
$\dot{\omega}$	.8748	.0361
$\dot{\Omega}$	-.4374	-.0181
$n + \dot{\omega} + \dot{\Omega}$ deg/day	1128.8443±.0001	285.1618±.0001
Mean Diameter, km	23.0	12.8
Gravitational Constant km^3/sec^2	2×10^{-3}	2×10^{-4}

and the adjacent star background with the other[2]. The center of figure of the natural satellite relative to the star background is then determined by fitting an ellipsoidal shape to the optical image. The center of the resulting ellipsoid is then assumed to be the center of mass. The two major sources of error are the basic pixel resolution and the center of mass determination within the image. To account for density inhomogenity and surface irregularities, it is assumed that this latter process has an error of 10% of the diameter of the natural satellite. Thus the total optical data error is modeled as the RSS of the 0.025 milliradian error and the 10% center determination error.

The strongest information source for determining the spacecraft orbital parameters is the DSN Doppler data. The actual data are counted Doppler frequency over a variable count time. The standard assumption is that the Doppler noise is white, which leads to an assumed Doppler error variance inversely proportional to the count time. For this analysis, the Doppler noise is assumed to be a conservative 1 mm/sec for a one minute count time.

Filter Algorithm. A sequential filter algorithm was used for this error analysis to permit a study of the evolution of the covariance during the close encounters. Keplerian orbital elements were taken as the state variables for both the spacecraft and the natural satellite. The mass of the particular natural satellite under consideration was appended as the thirteenth state variable.

The observational noise discussed above is seldom the limiting error source; for satellites of planetary bodies the limiting errors are due to uncertainties in the dynamic model. For a Viking spacecraft the dominant errors are the higher harmonics of the gravity field and the quasi-stochastic gas leaks from the spacecraft[7]. There are a variety of means of including such forces in the model[8]. For this study, the original Kalman approach[9] was adopted because of its simplicity; as will be shown later, this approach is consistent with more sophisticated models.

The pertinent equations are the observation equations

$$Y_k = H_k X_k + E_k,$$

the linearized dynamic model

$$X_{k+1} = \Phi_{k+1,\,k} X_k + C_{k,\,k+1} W_k,$$

the mapped covariance

$$P_{k+1}^{(-)} = \Phi_{k+1,\,k} P_k^{(+)} \Phi_{k+1,\,k}^T + C_{k,k+1} Q_k C_{k,\,k+1}^T,$$

the covariance update at the kth observation

$$P_k^{(+)} = (I - K_k H_k) P_k^{(-)},$$

and the Kalman gain

$$K_k = P_k^{(-)} H_k^T [H_k P_k^{(-)} H_k^T + R_k]^{-1}.$$

The dynamic noise on the twelve orbital elements was calculated by assuming a constant, random acceleration W_k between observations. The standard deviation of W_k was varied throughout the orbit and was calculated to be equivalent to a 1% error in the acceleration due to planetary oblateness at the satellite radius from Mars. Although current gravity fields[3,10,11] have formal statistics somewhat smaller than 1%, these fields are based on data from Mariner 9, which was somewhat insensitive to the gravity field of the northern hemisphere. Since the Viking orbiter has a northern hemisphere periapsis location, the 1% uncertainty was chosen to remain conservative. The state noise acceleration is bounded below by 10^{-11} km/sec^2 to account for quasi-stochastic gas leaks.

Spacecraft Orbit Determination Accuracy. The Viking navigation team has performed detailed studies of the orbit determination accuracies during the

nominal Viking mission period[7]. In order to test the validity of the model used for this extended mission study, the navigation team results were simulated. Figure 3 shows the results of this comparison. The steady state variation of the standard deviation in the spacecraft orbital elements throughout the Viking orbit on July 4, 1976, is compared with the uncertainties in the orbital elements as predicted by the navigation team. The team results (⊙) are based on batch processing of Doppler data from one hour after periapsis to

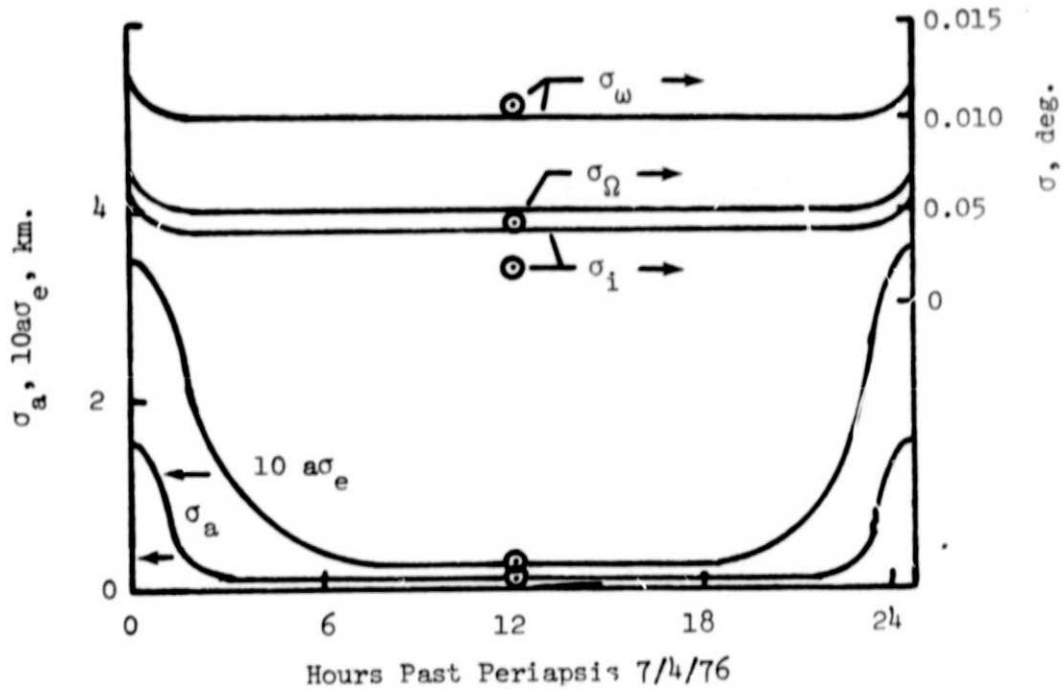

Figure 3. Comparison of Orbit Determination Results

one hour before the next periapsis. From this comparison, it was concluded that Kalman filter processing is sufficiently consistent to permit application of this filter model to the mass determination problem. The major source of positional error is an uncertainty of approximately 0.01 degrees in the nodal location in the plane of the sky coordinates. The resultant position error is therefore proportional to the distance of the spacecraft from the Mars-Earth line. Other positional error components are less than 1 km.

Natural Satellite Orbit Improvement. The uncertainties in the Keplerian elements, given in Table 1, indicate that the major positional error in 1976 will be an along-track error of about 30 km for Phobos and 80 km for Deimos.

To reduce this error, it is essential that optical imaging of the natural satellites be performed prior to the encounter attempt. Optical tracking of Deimos will actually be performed during the approach to Mars. It is expected that optical tracking of both satellites will be performed throughout the orbital phase of the nominal mission.

The sequential filter was used to obtain an estimate of the magnitude of the downtrack error after orbital phase imaging. Three images were simulated for each natural satellite during a single orbit in both July and December 1976. The resulting improvements in the along-track error are shown in Table 2.

Table 2

EFFECT OF ORBITAL PHASE OPTICAL DATA ON LONGITUDE ERROR (km)

	No Optical Data	July	December
Phobos	30	2.2	3.0
Deimos	80	1.8	1.1

No significant improvement in the other natural satellite orbital elements resulted from the optical data. It is assumed that July imaging has been performed. Thus, the subsequent analysis utilizes the satellite downtrack errors as given by the improved values.

Analytic Approximation to Mass Determination Accuracy. Anderson[12] introduced analytic approximations for the accuracy of determining the mass of an asteroid from a single spacecraft flyby. The significant assumptions were (1) that the spacecraft trajectory with respect to the asteroid is a rectilinear hyperbola and, (2) that the only trajectory parameter included in the estimation process is the distance of closest approach. Based on these assumptions the variance of the estimate of the mass parameter is

$$\sigma^2 (GM \sin i) = 16bv^3 \tau\sigma^2 (\dot{\rho})/\pi \qquad (1)$$

If it is further assumed that the distance of closest approach is known, the estimate variance becomes

$$\sigma^2 (GM \sin i) = 2bv^3 \tau\sigma^2 (\dot{\rho})/\pi \qquad (2)$$

In the above formulas, GM is the gravitational constant of the asteroid, i is the inclination of the flyby hyperbola to the plane of the sky, b is the distance of closest approach, v is the relative velocity, τ is the Doppler count time, $\sigma^2(\dot{\rho})$ is the variance on the Doppler velocity measurement. Under the basic assumptions of Anderson's analysis, it is impossible to separate GM and sin i, the well-known spectroscopic binary star result.

The Viking encounters with Phobos and Deimos occur over such a short time span that the above approximations are applicable, producing insight into the optimal geometry and expected results. It should be noted that the relative velocity is essentially invariant for the degrees of freedom available in designing the encounter sequence[1]. Also, the assumption on the Doppler noise makes the term $\tau\sigma^2(\dot{\rho})$ a constant. These parameters are therefore not available for optimizing the experiments. However, assuming that the inclination to the plane of the sky can be determined from the known orbits of the satellites, it is clear that GM is best determined from close encounters with 90° inclinations to the plane of the sky.

Phobos Mass Determination During the January Encounter Opportunity. It has been shown[1] that small variations in the phasing and synchronization maneuvers permit substantial variations in the encounter geometry. Thus, these maneuvers can be used to optimize the encounter sequence to provide the best mass determination accuracy. Figure 4 shows 2 sets of encounters for the January Phobos opportunity. These sequences are based on the 1 to 3 synchronized orbits discussed earlier. Each circle in the figure represents a point where the spacecraft descends through the Phobos orbital plane. The components of the spacecraft velocity relative to Phobos are -1.68, 0.42, and -1.1 km/sec. The Earth is about 6° south of the orbital plane in the direction shown.

The set of encounters represented by open circles (set I) is designed so that each encounter passes nearly through the Phobos-Earth line, thus maximizing the inclination to the plane of the sky. As seen in Fig. 5, this design produces only two encounters which pass within 100 km of Phobos. The encounter set represented by closed circles (set II) is designed to maximize the number of close approaches without regard for the inclination to the plane of the sky. The intersection points are designed to form a line parallel to the

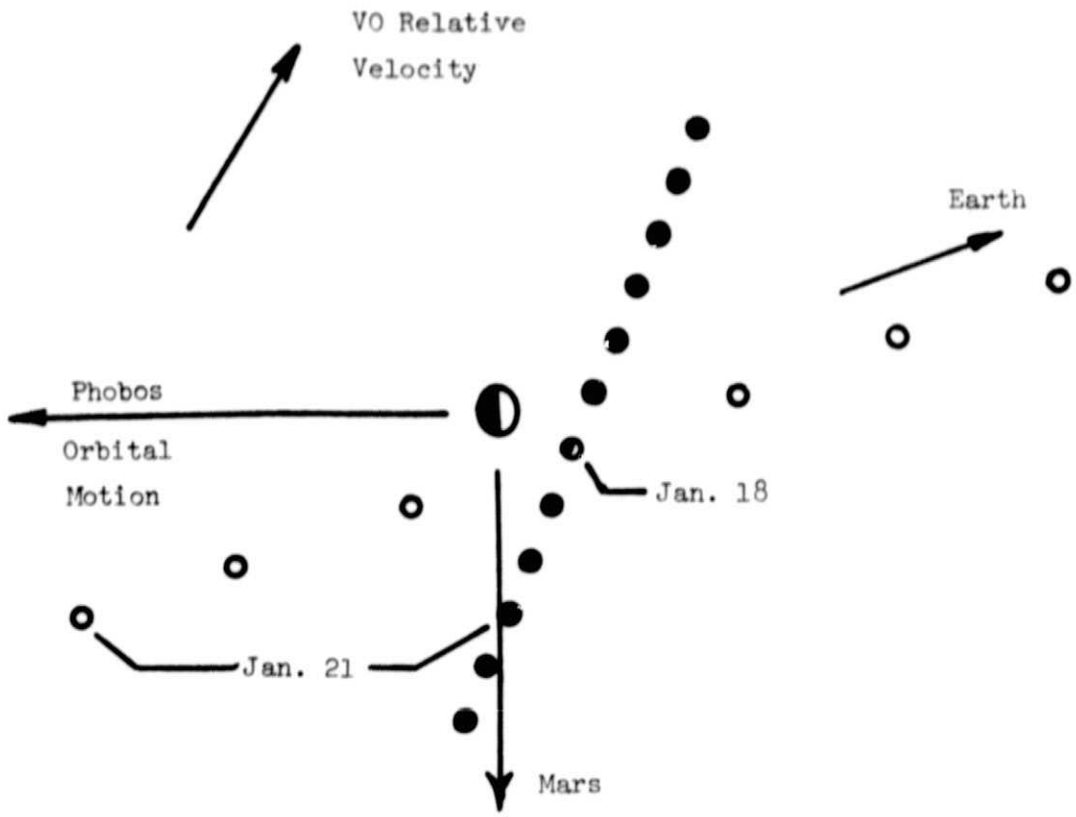

Figure 4. Phobos Encounter Geometry in January

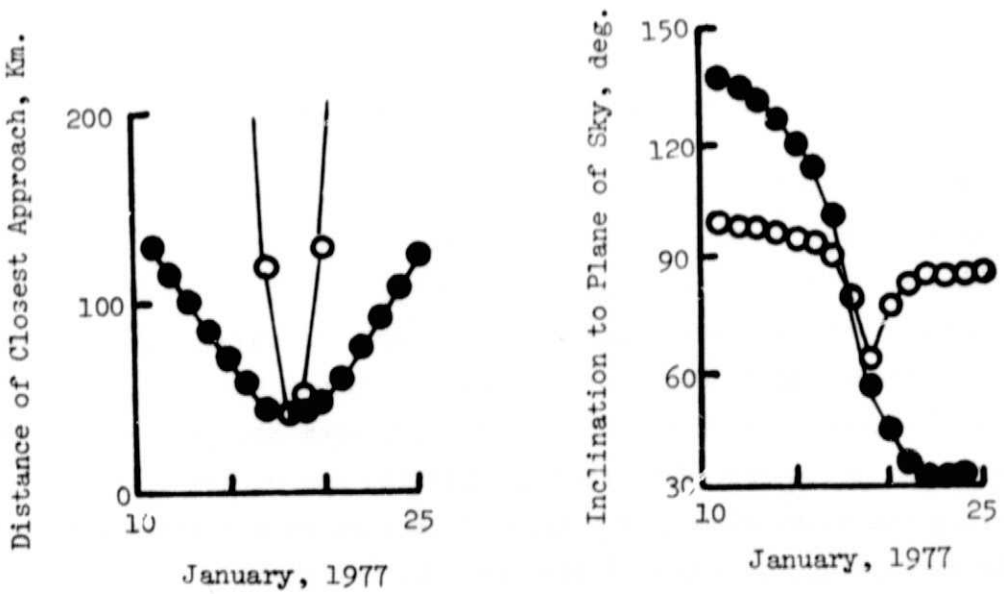

Figure 5. Phobos Encounter Parameters in January

relative velocity vector. This results in 9 encounters which pass within 100 km of Phobos.

Both of these encounter sets were analyzed using the sequential filter discussed above. Results of the error analyses for both encounter sets are presented in Fig. 6. The satellite mass a priori was set equal to the nominal estimate in Table 1. Encounter set II clearly provides the quickest improvement in the knowledge of the satellite mass due to the large number of close encounters. However, the final uncertainty is about the same for both sets.

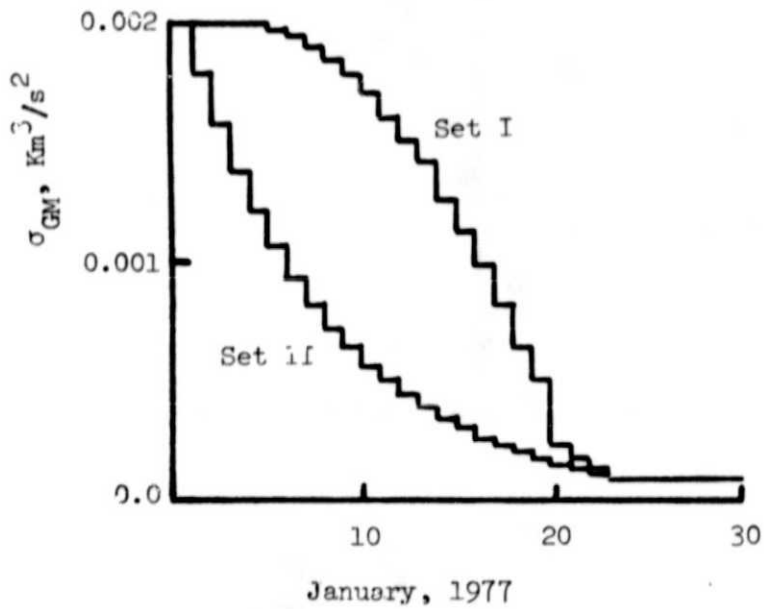

Figure 6. Multi-Orbit Mass Determination

Neither set provides any substantial improvement in the Phobos orbital elements. The stairstep nature of the mass improvement indicates that very little information on the mass remains in the Doppler data after the spacecraft has receded from the natural satellite. Simple calculations show that for a spacecraft-Phobos distance of over a few thousand kilometers, there is no observable direct Doppler shift. Therefore, improvements in the mass after the encounters must arise from correlations with the spacecraft state variables, developed during the close encounter phase. A lack of such improvement could be due to the corrupting influence of the Mars gravity field.

To confirm this assertion, the orbit in set II which came within 40 km of Phobos was analyzed. During the encounter, large correlations are developed between the Phobos mass and all six spacecraft elements. After the encounter, the general variation of each correlation is fairly well illustrated by Fig. 7, in which the correlation between mass and semimajor axis is presented. The solid curve corresponds to the nominal case where the dynamic noise is based on a 1% error in J_2 and a non-gravitational acceleration of 10^{-11} km/sec^2. The short dashed line corresponds to the case in which the gravity field is known perfectly. The third case results from a perfectly known gravity field

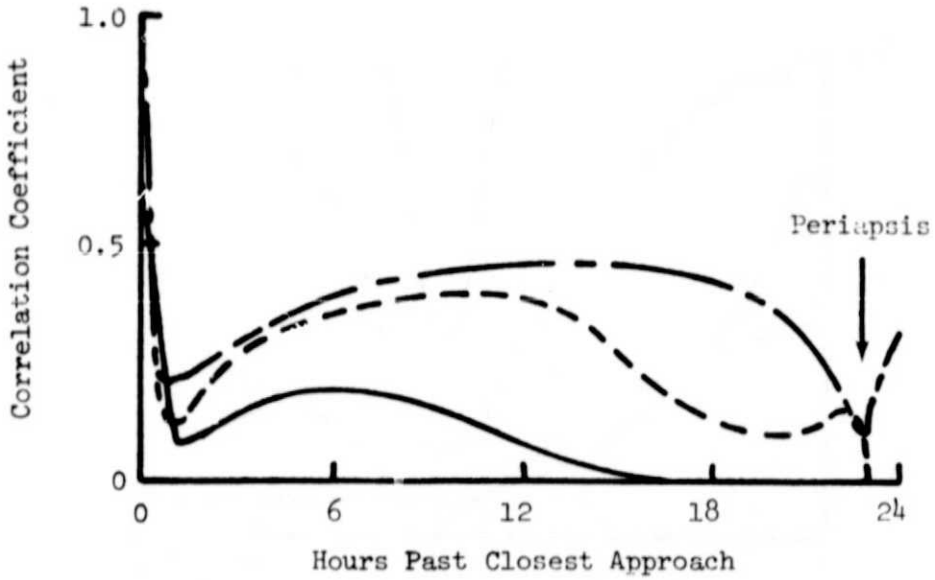

Figure 7. Evolution of Correlations

and a non-gravitational acceleration of 10^{-13} km/sec^2. The uncertainty in the gravity field causes the filter to "forget" the encounter well before the next periapse passage. Non-gravitational forces at the 10^{-11} level reduce the correlations to .06 at the next periapsis. A nearly perfect dynamic model is required before information is propagated around to the next encounter. Therefore, processing multi-orbits in a continuous mode may provide no advantage over processing single orbits in a multi-batch mode.

A multi-batch process was simulated by applying the sequential filter to each encounter within set II as if none of the other encounters in that set existed. The results of this analysis are presented in Fig. 8. Each point represents the steady state value of the mass standard deviation after the spacecraft has receded from Phobos. The analytical estimates on the standard deviation given by equations (1) and (2) above can be directly applied to this filter strategy. The Kalman results are seen to be between the analytic bounds, and the general shape of the curves agree well. Thus, the analytic formulas provide a computationally efficient tool for future optimization of the encounter sequence.

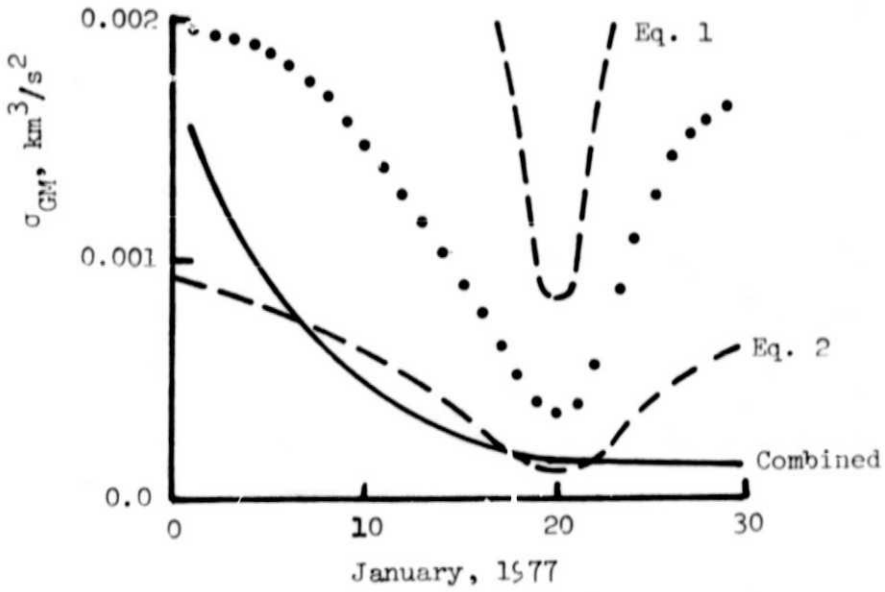

Figure 8. Single-Orbit Mass Determination

Statistically combining these individual Kalman covariances in a sequential manner provides the lower curve in Fig. 8. A comparison of this result with Fig. 6 confirms that a multibatch process is essentially as accurate as the single long arc, multi-orbit process. Since the multi-batch strategy permits further optimization with respect to filter parameters, this approach will probably be the optimal method for the January encounter.

Phobos March Encounter. The March encounter sequence with Phobos was designed to maximize the number of close encounters. The locations of the intersection points with the Phobos orbital plane are shown in Fig. 9; there are 9 encounters within 100 km of Phobos. Figure 10 shows a large variation in the inclination to the plane of the sky.

The evolution of the mass standard deviation is presented in Fig. 11. The final standard deviation in January is 3/2 larger than the March result. This slight improvement is brought about by the change in the location of the Earth. Recall that the major uncertainty in the spacecraft position is produced by a rotation of the orbit about the Mars-Earth line. During the January encounters the spacecraft is about 9,000 km from this line, whereas in March this distance is only 4,400 km. Thus, the relative position of Phobos and the spacecraft is slightly better determined in March, which permits the improvement.

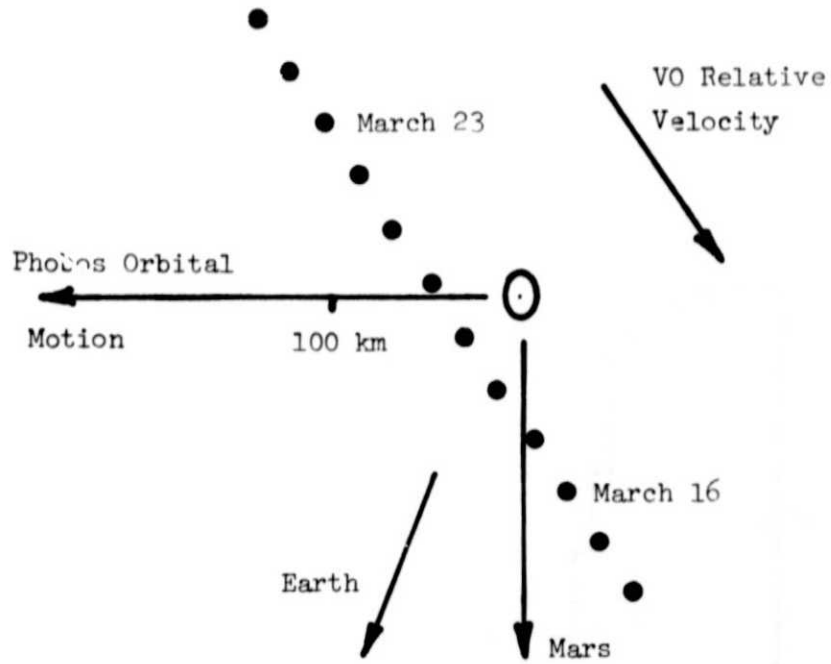

Figure 9. Phobos Encounter Geometry in March

Deimos Encounter. It is assumed that the spacecraft has been maneuvered into a 1-to-1 synchronization with Deimos to provide the maximum number of close encounters. This is essential, since the Deimos encounters occur at over three times the distance from Mars as the Phobos encounters. This causes

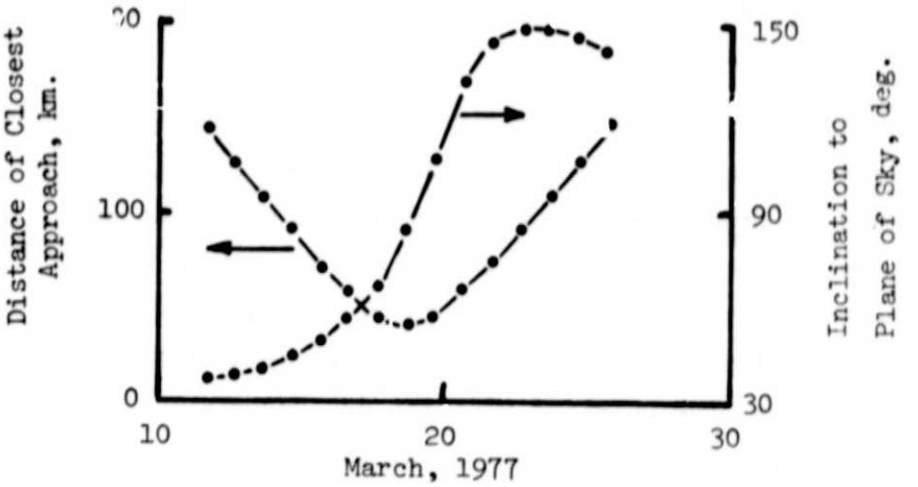

Figure 10. Phobos Encounter Parameters in March

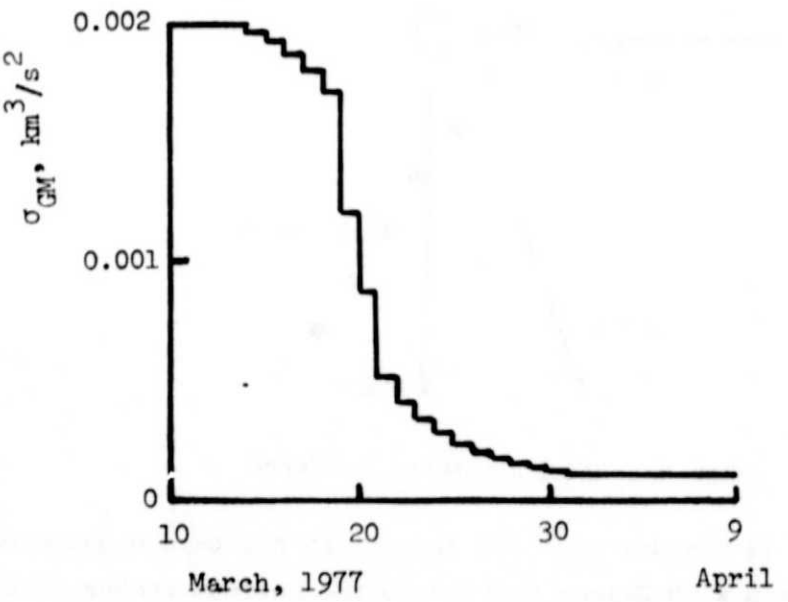

Figure 11. Multi-Orbit Mass Determination in March

the spacecraft intersection points within the Deimos orbital plane to move over three times farther radially per spacecraft orbit. The number of close encounters will therefore be limited, even in the optimal case which is illustrated in Fig. 12. There are only 5 encounters within 100 km as illustrated in Fig. 13. The closest encounter, at 30 km, has a relatively high inclination to the plane of the sky. In addition, this encounter is only 7500 km off the Mars-Earth line, even though the Deimos encounter phase occurs at 23,000 km from Mars. Thus, the relative positions of the spacecraft and Deimos are better determined than those of the January-Phobos encounter.

The evolution of the Deimos mass standard deviation is presented in Fig. 14. The final uncertainty is 25% of the a priori estimate of the total mass. Almost all of the improvement comes from the encounters on Nov. 29 and 30. To determine the contribution of each encounter, the closest encounters in this sequence were reanalyzed in the single encounter mode. These results are also presented in Fig. 14. These are the only two encounters which provide better than 50% mass determination.

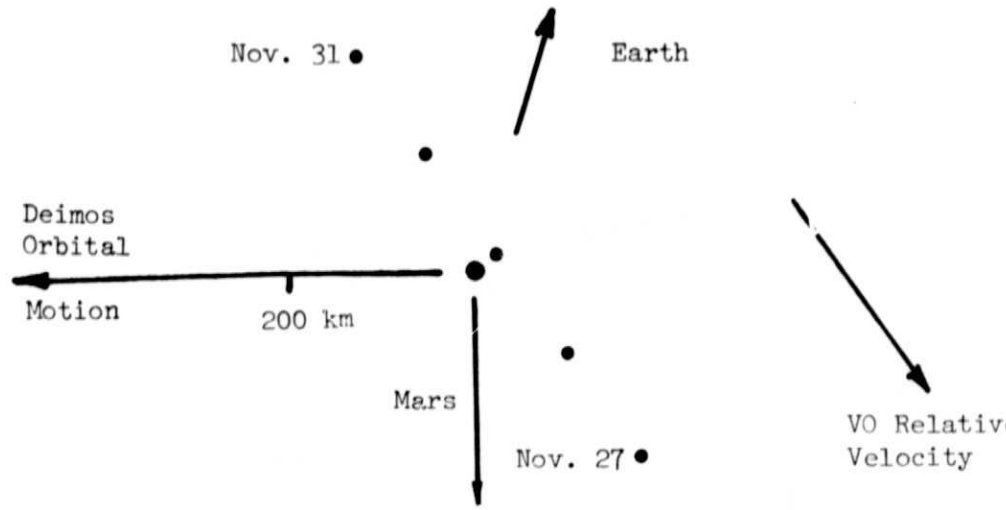

Figure 12. Deimos Encounter Geometry

The above analysis is based on the 1-to-1 synchronization between orbital periods, which may require a propulsive expenditure of about 50 m/s. A 4-to-5 orbital period ratio can be established for less than 5 m/s. However, such suboptimal encounter sequences provide only one close encounter, limiting the accuracy of the mass determination to about 35%. In addition, these sequences do not provide independent estimates of the mass.

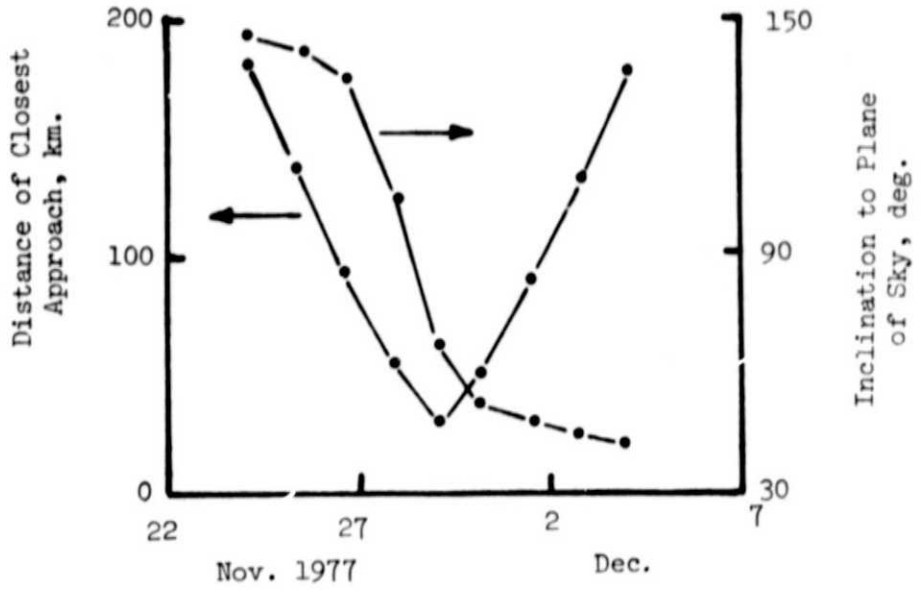

Figure 13. Deimos Encounter Parameters

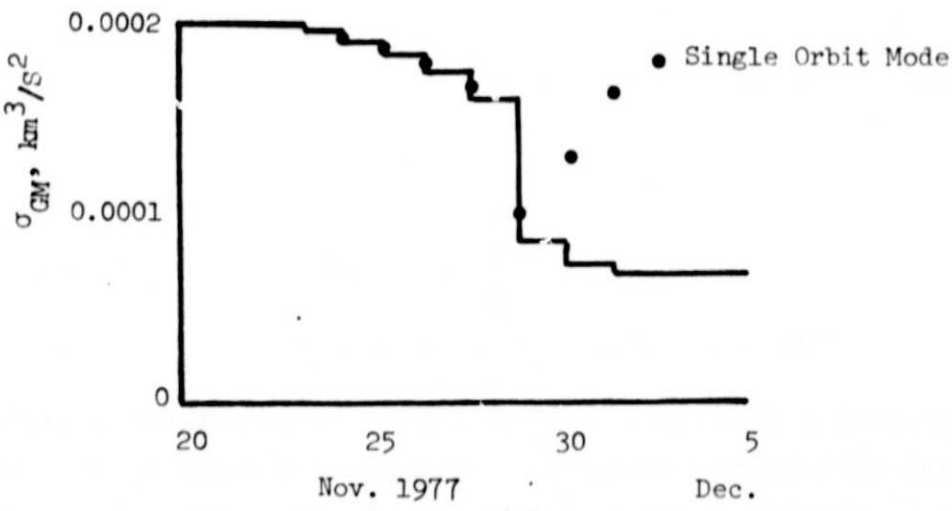

Figure 14. Deimos Mass Determination

Probability of Collision with Phobos and Deimos. Determining the mass of the natural satellite depends strongly on the minimum distance of closest approach. This distance must be sufficiently large to assure a low probability of spacecraft impact. The impact probability has been determined by assuming that the encounter geometries are those discussed earlier. Based on the spacecraft and satellite orbit determination accuracies at closest approach minus 1, 2, and 5 orbits, the probability of impact during the closest encounter was calculated using a Monte Carlo technique with 10,000 samples. The results are presented in Table 3.

Table 3

Percent Impacts	Orbits to Closest Approach		
	5	2	1
January	7.2	7.8	1.4
March	2.4	0.7	0.1
November	3.1	1.4	1.0

To assure an impact probability of less than 1% will require a decision one orbit prior to the closest encounter except in March, when a reduced collision probability results from the previously discussed improvement in spacecraft determination.

A simulation was also performed for the January case exclusing the downtrack improvement afforded by the optical data. The probability of collision was increased from 1.4% to 3.8%. Thus, optical data plays an important role in the design of close encounters.

CONCLUDING REMARKS

The application of a Kalman filter to the Phobos and Deimos encounter opportunities during the Viking extended mission has shown that the mass of Phobos can be determined to the 10% level, during either the January or March (1977) opportunities. The Deimos mass can be determined to about 25% with the optimal encounter geometry, which provides two close encounters. This uncertainty is increased to about 35%, if only one close encounter is possible.

SYMBOLS

a	semimajor axis of Keplerian orbit, km
b	distance of closest approach, km
$C_{k, k+1}$	state noise transition matrix
e	eccentricity of Keplerian orbit
E_k	observation noise vector
GM	product of gravitational constant and mass of central body, km^3/sec^2
H_a	altitude of apoapsis, km
H_p	altitude of periapsis, km
H_k	observation matrix
i	orbital inclination, deg
I	identity matrix
J_2	planetary oblateness coefficient
K_k	Kalman gain matrix
M_o	mean anomaly
n	mean motion, sec^{-1}
P_k	covariance matrix
$Q_{k+1, k}$	state noise covariance matrix
R	mean radius of Mars, km
R_k	observational noise covariance matrix
v	relative velocity, km/sec
W_k	random acceleration
X_k	state vector
Y_k	observational vector
σ_x^2	variance on parameter x
$\sigma^2(\dot{\rho})$	variance on the Doppler velocity measurement, $(km/sec)^2$
τ	Doppler count time, sec
ω	argument of periapsis, deg

Ω	longitude of ascending node of Keplerian orbit, deg

Subscripts:

k	kth observation

Superscripts:

T	transpose
-1	inverse
(-)	prior estimate
(+)	updated estimate

A dot over symbol denotes differentiation with respect to time.

REFERENCES

1. R. H. Tolson; R. C. Blanchard and E. F. Daniels: "Phobos and Deimos Encounter Experiment During the Viking Extended Mission," AIAA 13th Aerospace Sciences Meeting, January 20-22, 1975, Pasadena, California.

2. T. C. Duxbury: "Phobos and Deimos Geodesy," I.A.U. Colloquium #28 Planetary Satellites, Ithaca, New York, August 18-21, 1974.

3. G. H. Born: "Mars Physical Parameters as Determined From Mariner 9 Observations of the Natural Satellites and Doppler Tracking," JGR, Vol. 79, No. 32, November 10, 1974.

4. J. B. Pollack, et al.: "Mariner 9 Television Observations of Phobos and Deimos II," JGR, Vol. 78, No. 20, July 10, 1973.

5. G. A. Wilkins: "A New Determination of the Elements of the Satellites of Mars," Theory of Orbits in the Solar System and in Stellar Systems, edited by G. Contopoulos, pp. 271-273, Academic, New York, 1966.

6. A. T. Sinclair: "The Motions of the Satellites of Mars," Mon. Notic. Roy. Astron. Soc., Vol. 155, No. 249-274, 1972.

7. Viking 1975 Navigation Plan, Vol. II, May 1, 1975.

8. K. G. Myers and B. D. Tapley: "Dynamical Model Compensation for Near-Earth Satellite Orbit Determination," AIAA Journal, Vol. 13, No. 3, March 1975.

9. R. E. Kalman: "A New Approach to Linear Filtering and Prediction Problems," Journal of Basic Engineering, March 1960.

10. R. D. Reasenberg; I. I. Shapiro and R. D. White: "The Gravity Field of Mars," GRL, Vol. 2, No. 3, March 1975.

11. J. Lorell, et al.: "Gravity Field of Mars From Mariner 9 Tracking Data," Icarus, Vol. 18, No. 304, 1973.

12. J. D. Anderson: "Feasibility of Determining the Mass of an Asteroid From a Spacecraft Flyby," Physical Studies of Minor Planets, NASA, Washington, D. C., 1971.